Numerical investigation of the real and ideal gap profiles in the calculation of the pressure distortion coefficient and piston fall rate of an LNE 200 MPa pressure balance

P Wongthep[1,2], T Rabault[1], R Noguera[2] and C Sarraf[2]

[1] Laboratoire National de Métrologie et d'Essais (LNE), 1, rue Gaston Boissier, 75724 Paris Cedex 15, France
[2] Laboratoire de dynamique des Fluides, Ecole doctorale, Arts et Métier Paristech, 151, bd de l'Hôpital, 75013 Paris, France

E-mail: padipat.wongthep@lne.fr

Abstract
This paper aims to investigate, by means of numerical simulation, the effect of gap profiles on the calculation of the pressure distortion coefficient (λ) and the piston fall rate (v_f) of two piston–cylinder units used in a Laboratoire National de Métrologie et d'Essais (LNE) 200 MPa pressure balance. The ideal mean gap width between the piston and the cylinder was obtained after measuring the piston fall rate at a low pressure, while the piston radius was obtained from the cross-float experiments at a low pressure. The real gap width was obtained from dimensional measurements by measuring the diameter and straightness of the piston and the cylinder. The piston and cylinder radial distortions were calculated using the finite element method. The pressure distribution in the gap was calculated on the basis of the Navier–Stokes equation for Newtonian viscous flow. The results such as pressure distributions, radial distortions, the pressure distortion coefficient and the piston fall rate were presented for the free-deformation operating mode of the assemblies. The calculation resulted in ideal and real gap profiles indicating that the average pressure distortion coefficient was in good agreement within $0.017 \times 10^{-6}\,\mathrm{MPa}^{-1}$ and the calculations of piston fall rate depended on the gap profile especially at the inlet and outlet zones of the engagement length.

1. Introduction

Pressure balances are used in many national metrology institutes (NMIs) as primary pressure standards from a few kilopascals up to approximately 1 GPa. The pressure balance consists of a loaded piston inserted into a closely fitted cylinder. The effective area (A_p) of the piston–cylinder unit (PCU) is commonly defined as a function of the effective area at zero pressure (A_0), the pressure applied (p) and the pressure distortion coefficient (λ):

$$A_p = A_0(1 + \lambda p). \tag{1}$$

For pressures above 50 MPa, λ contributes significantly to the final uncertainty budget. That is why its evaluation is so critical and many studies have been carried out on this subject [1–4]. Other studies include EUROMET projects No 256 [5] and 463 [6], which were organized from 1994 to 2006 to compare the results of laboratories' calculations of λ using the finite element method (FEM). In the first project, a 400 MPa PCU of the Physikalisch-Technische Bundesanstalt (PTB) and two 200 MPa PCUs of LNE, the latter identified by N°4 and N°5, were selected to compare the calculations by assuming that the gaps between the piston and the cylinder were constant (ideal gap) along the engagement length. In the second project, a 1 GPa PCU of PTB was selected for calculations and the real geometry of the piston and the cylinder (real gap) was taken into account. The results of the last project showed that

the difference in λ obtained from the ideal and real gaps lay between $0.057 \times 10^{-6}\,\mathrm{MPa}^{-1}$ and $0.080 \times 10^{-6}\,\mathrm{MPa}^{-1}$.

The objective of this work was to investigate the difference in calculations of λ and v_f between the ideal and real gap profiles of the LNE 200 MPa PCUs N°4 and N°5 in order to understand the effect of the gap profile between the piston and the cylinder especially at the inlet and outlet gaps.

2. Design and properties

The PCUs under investigation are LNE 200 MPa manufactured by Desgranges et Huot (DH), France. These PCUs can be mounted in the pressure balance for the pressure scale from 6 MPa to 200 MPa, with a load from 30 kg to 1000 kg, and operate in either free-deformation (FD) or controlled-clearance mode. EUROMET project No 256 [5] used the same PCUs to calculate the pressure distortion coefficient for the ideal constant gap between the piston and the cylinder. The basic geometry is shown in figure 1. Both the piston and the cylinder are made of tungsten carbide with 6% of cobalt. The material properties of the piston and the cylinder given by the manufacturer are as follows:

$$\text{Young's modulus } (E) \ = 628\,\mathrm{GPa}$$

$$\text{Poisson's coefficient } (\mu) \ = 0.218.$$

The expanded uncertainties claimed by the manufacturer are 5% and 2% for E and μ, respectively. In the pressure balance, diethyl-hexyl-sebacate (DHS) is used as a pressure-transmitting fluid. The density (ρ) and the dynamic viscosity (η) were measured experimentally [7]. The values of ρ and η depend on pressure p and, at 20 °C, can be determined by the following equations:

$$\rho/(\mathrm{kg\,m^{-3}}) = 912.6657 + 0.752\,097\,p - 1.644\,85 \times 10^{-3}\,p^2 + 1.456\,25 \times 10^{-6}\,p^3 \quad (2)$$

$$\eta/(\mathrm{Pa\,s}) = 0.021\,554\left(1 + 1.900\,36 \times 10^{-3}\,p\right)^{8.8101} \quad (3)$$

where p is given in MPa. The relative standard uncertainty of ρ and η is 1%.

The piston–cylinder assembly has an engagement length (l) of 40 mm and a nominal effective area of 50.3 mm^2. From measurements of the piston fall rate (v_f) at low pressure, the mean gap width between the piston and the cylinder (h_0) at zero pressure was found after extrapolating the piston fall rate. The mean gap width (h) at measurement pressure p is described by the equation

$$h^3 = 6 r_0 v_f \eta \frac{l}{p}. \quad (4)$$

The values of h_0 for the 200 MPa PCUs N°4 and N°5 were found, respectively, to be

$$h_0 = (0.540 \pm 0.044)\,\mu\mathrm{m}$$

$$h_0 = (0.272 \pm 0.028)\,\mu\mathrm{m}.$$

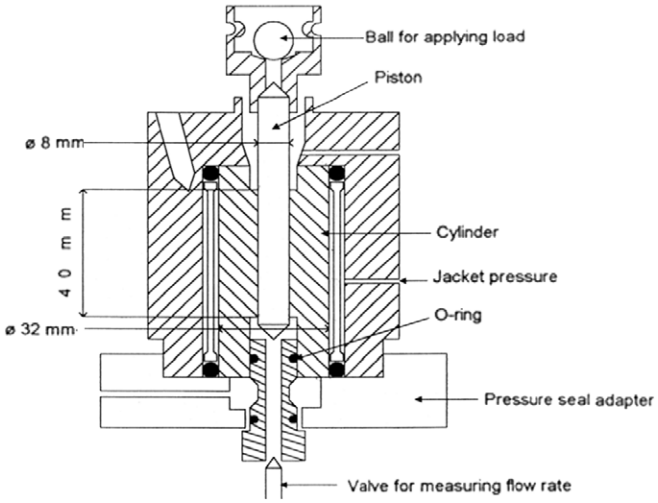

Figure 1. LNE 200 MPa piston–cylinder assembly.

For each PCU, the mean piston radius (r_0) and the mean cylinder radius (R_0) were calculated from A_0 that was obtained from the cross-float experiments at a low pressure and h_0. The mean radii r_0 and R_0 of the 200 MPa PCU N°4 were calculated to be

$$r_0 = (4.000\,143 \pm 0.000\,030)\,\mathrm{mm}$$

$$R_0 = (4.000\,683 \pm 0.000\,030)\,\mathrm{mm}.$$

The mean radii r_0 and R_0 of the 200 MPa PCU N°5 were calculated to be

$$r_0 = (4.000\,116 \pm 0.000\,025)\,\mathrm{mm}$$

$$R_0 = (4.000\,388 \pm 0.000\,025)\,\mathrm{mm}.$$

The mentioned uncertainties for h_0, r_0 and R_0 are expanded uncertainties.

Dimensional measurements on the piston and the cylinder were made by the dimensional department at LNE. The measurements included determination of diameters and straightness data. The diameters of the piston and the cylinder were measured in two orthogonal directions (0° and 90°) at three horizontal levels for the 200 MPa PCU N°4 as well as at five horizontal levels for the PCU N°5, and then were used as reference points for converting the straightness data along the axial coordinate. The straightness data were obtained from four different angles (0°, 90°, 180° and 270°) varying on the axial coordinate with an incremental step of 0.1 mm.

According to the information obtained from the dimensional department, the expanded uncertainty of the piston and cylinder radii ($r = r_z$ and $R = R_z$) is equal to 40 nm. The maximum error of the gap conicity is equal to 2 $\mathrm{nm\,mm^{-1}}$ (obtained by averaging the data of the dimensional measurements) for each PCU.

3. Models and conditions

The analysis used the finite element model as defined in figure 2 and table 1. The piston and cylinder were assumed to be

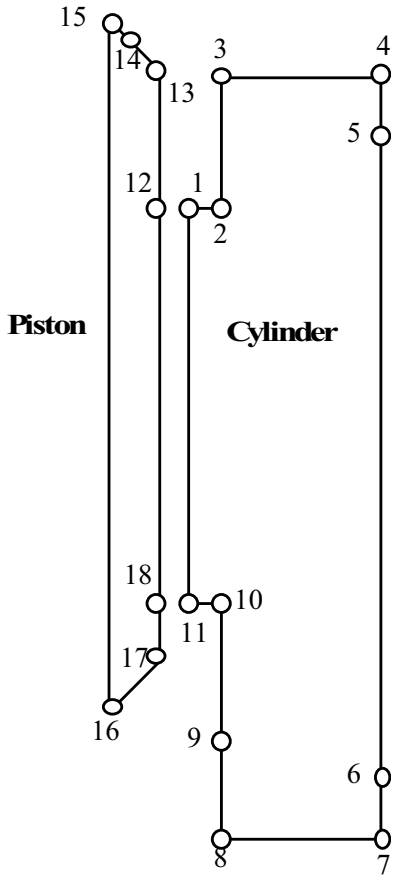

Figure 2. Model of the PCU 200 MPa.

Table 1. Keypoint coordinates of the PCU 200 MPa.

Keypoint	x/mm	z/mm	Keypoint	x/mm	z/mm
1	R_z	62	10	4.2	22
2	4.2	62	11	R_z	22
3	4.2	67	12	r_z	62
4	16	67	13	r_z	91
5	16	62	14	1	$91 + (r_z - 1)\tan 60$
6	16	22	15	0	$91 + r_z \tan 60$
7	16	0	16	0	$15 - r_z \tan 60$
8	4.2	0	17	R_z	15
9	4.2	5.2	18	R_z	22

axisymmetric, allowing the use of a two-dimensional model, with a constant gap and a real gap along the engagement length. The radii r_z and R_z in table 1 correspond to the axial coordinate.

Figure 2 identifies the location of the keypoints of the PCUs at which specific boundary conditions were applied. Lines 3–4 and 13–15 were prevented from moving in the axial direction and line 15–16 in the radial direction. The measured pressure (p) was applied on lines 9–10, 10–11, 16–17 and 17–18. Lines 1–11 and 12–18 were loaded by the gradient pressure (p_z) in the gap.

4. Numerical approach and calculation methods

Numerical calculations were performed with the ANSYS-Parametric Design Language (APDL), which allowed the application of the FEM. This study used a mesh of eight-node quadrilateral elements (named PLANE183 in the APDL) of different size with a higher concentration at the two faces along the piston–cylinder engagement length. Different meshes were tested to find the optimal results, which were obtained by using 1235 elements on the PCU and 163 element faces along the piston–cylinder engagement length.

A common method for determining the distortion was a separate solution of the fluid flow and structural problem. The fluid flow was analysed in the annular gap, which was affected by structural distortions. The annular wall distortions were determined iteratively after carrying out an FEM structural analysis. The pressure distribution obtained after analysing the fluid flow was, at the same time, used as the load condition in the structure problem. The solution of the two coupled problems was determined through structural and fluid flow analyses that were performed iteratively until a convergence of the output parameters of interest was obtained. The convergence criterion was a relative change in the pressure distribution in the last and the previous iteration of less than 10^{-10} and in the deformation of less than 10^{-6}.

Assuming that the geometry of the PCU and the applied pressure load were axisymmetric, and the piston and the cylinder were in elastic equilibrium, the stress–strain distribution was obtained numerically using the FEM and allowed radial displacements of the piston and cylinder, $u_z(p_z)$ and $U_z(p_z)$ respectively, and the gap width, $h_z(p_z) = R_z(p_z) - r_z(p_z)$, to be determined.

The equilibrium of the PCU is a condition that is usually applied to fluid dynamics laws. Therefore, the velocity profile of the fluid moving through a gap between the piston and the cylinder as a function of variation in pressure at both ends of the piston–cylinder engagement length of the PCU can be determined by applying the Navier–Stokes equation [8]. Assuming that the liquid is Newtonian and has a low compressibility, and that the fluid flow is stationary, isothermal, laminar and one-dimensional, then the mass force is negligible compared to the viscous force. The mass flow (Q_m) through the gap between the piston and the cylinder can be evaluated by taking into account the variable fluid characteristics (ρ and η) in the gap between the piston and the cylinder:

$$Q_m = \frac{\pi r h_z^3 \rho(p_z)}{6\eta(p_z)} \frac{\mathrm{d}p_z}{\mathrm{d}z} \tag{5}$$

and the piston fall rate (v_f) was calculated from the following equation:

$$v_\mathrm{f} = \frac{Q_m}{\pi r^2 \rho(p)}. \tag{6}$$

The pressure distribution (p_z) can be calculated using equation (5) under the assumption that Q_m is constant along the whole engagement length:

$$p_z = p \left\{ 1 - \frac{\displaystyle\int_0^z \frac{\eta(p_z)}{\rho(p_z)h_z^3}\,\mathrm{d}z}{\displaystyle\int_0^l \frac{\eta(p_z)}{\rho(p_z)h_z^3}\,\mathrm{d}z} \right\}. \tag{7}$$

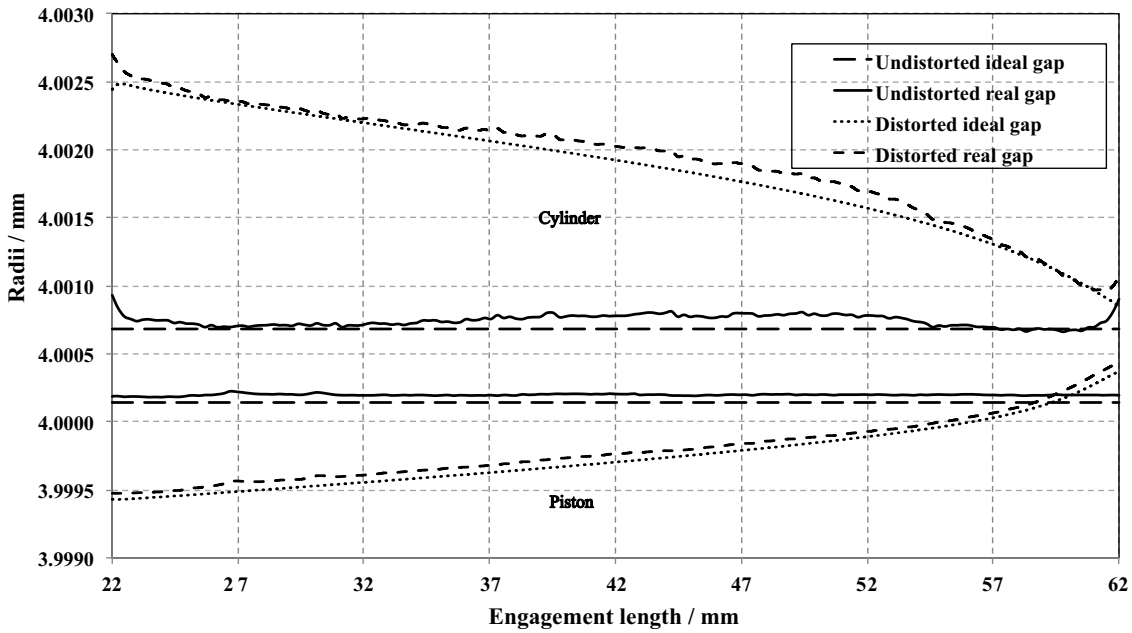

Figure 3. Undistorted and distorted gap profiles of the piston and the cylinder in the FD mode for the 200 MPa PCU N°4 at $p = 200$ MPa.

After obtaining $r_z(p)$, $R_z(p)$ and p_z, the effective area (A_p) can be determined by balancing the action of axial forces on the piston, according to [9], as

$$A_p = \pi r_0^2 \left[1 + \frac{h_0}{r_0} + \frac{1}{r_0 p} \int_0^l p_z \frac{d\,(u_z + U_z)}{dz} dz \right]. \quad (8)$$

All parameters in equation (8) are dependent on p_z. The effective area at zero pressure (A_0) can be calculated as follows:

$$A_0 = \pi r_0^2 \left[1 + \frac{h_0}{r_0} + \frac{1}{r_0} \frac{\int_0^l \frac{(u_z + U_z)}{h_z^3} dz}{\int_0^l \frac{1}{h_z^3} dz} \right] \quad (9)$$

and the effective area at zero pressure (A_0) in the case of an ideal gap profile is given by

$$A_0 = \pi r_0^2 \left[1 + \frac{h_0}{r_0} \right]. \quad (10)$$

5. Results

The pressure distortion coefficients and the piston fall rates were calculated at the measured pressure $p = 20$ MPa, 70 MPa, 120 MPa, 160 MPa and 200 MPa in the FD mode and a reference temperature of 20 °C. In this calculation, the number of iterations depended on the measured pressure. The calculations were performed iteratively until satisfactory convergence was obtained, which was, e.g., 23 iterations for the calculation of pressure distribution and 25 iterations for gap deformation at the maximum pressure.

The results of the distorted gap between the piston and the cylinder along the engagement length are shown in figures 3 and 4 for the 200 MPa PCUs N°4 and N°5, respectively. Both results were obtained at the measured pressure $p = 200$ MPa in the FD mode. The calculations of the distorted cylinder obtained from the ideal and real gap profiles were different at the inlet and outlet gaps for both PCUs. The distortions of the piston obtained from the ideal and real gaps were in good agreement for both PCUs.

The pressure distribution along the engagement length for the two assemblies and two models is given in figure 5. The results show that the pressure distributions in the gap depend not only on the measured pressure but also on the gap width. The pressure distribution is non-linear and increases with the measured pressure. The biggest difference between the two gap profiles can be seen at the zone near the gap exit.

The calculated pressure distortion coefficients are given in table 2. For the ideal gap of the two assemblies, there is no significant difference in the range from 20 MPa to 200 MPa, and the maximum variation is only 0.05×10^{-7} MPa^{-1} for the 200 MPa PCU N°4. For the real gap, the variations are 0.18×10^{-7} MPa^{-1} and 0.21×10^{-7} MPa^{-1} for the 200 MPa PCUs N°4 and N°5, respectively. The maximum differences of pressure distortion coefficients obtained from the ideal and real gap profiles are 0.25×10^{-7} MPa^{-1} and 0.18×10^{-7} MPa^{-1} for the 200 MPa PCUs N°4 and N°5, respectively. The results of λ are shown graphically in figure 6.

The results of the piston fall rate calculations are plotted in figure 7 and listed in table 2. For the higher pressure, the piston fall rate values obtained for the ideal and real gaps were found to be 8.016 µm s^{-1} and 7.993 µm s^{-1}, respectively, for the 200 MPa PCU N°4. The results for the 200 MPa PCU N°5 amounted to 4.989 µm s^{-1} and 6.150 µm s^{-1} for the ideal and real gap profiles, respectively. The differences in results between the calculations of the piston fall rate for the ideal and real gap profiles depend on the measured pressure and also on their inlet and outlet gaps. The piston fall rates calculated for the 200 MPa PCU N°4 are higher than those for the 200 MPa PCU N°5 because of the larger gap width of the former. The

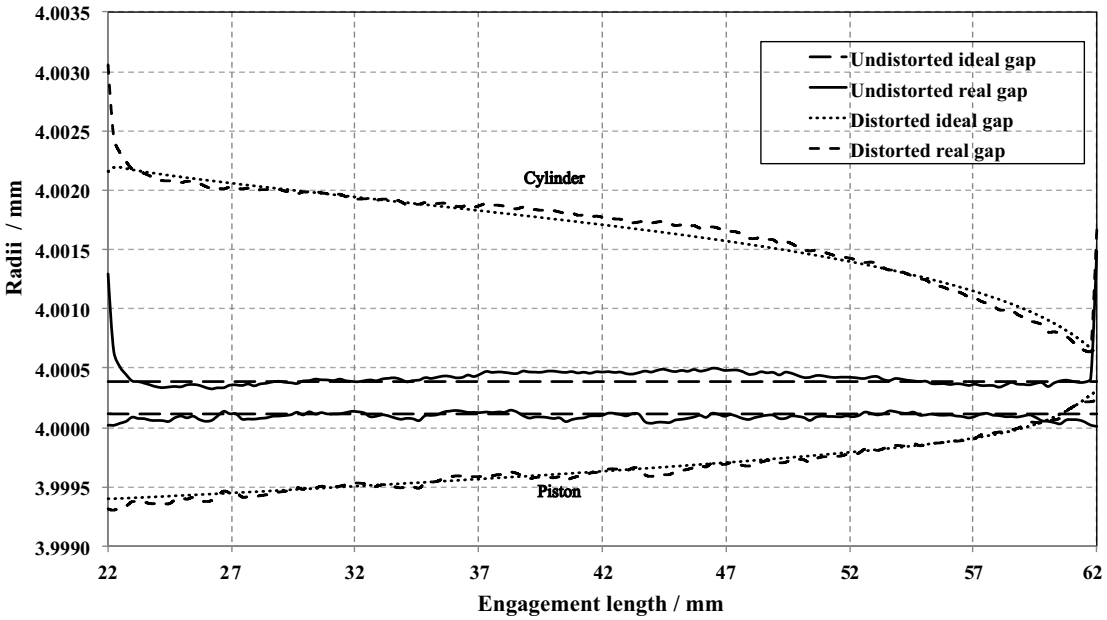

Figure 4. Undistorted and distorted gap profiles of the piston and the cylinder in the FD mode for the 200 MPa PCU N°5 at $p = 200$ MPa.

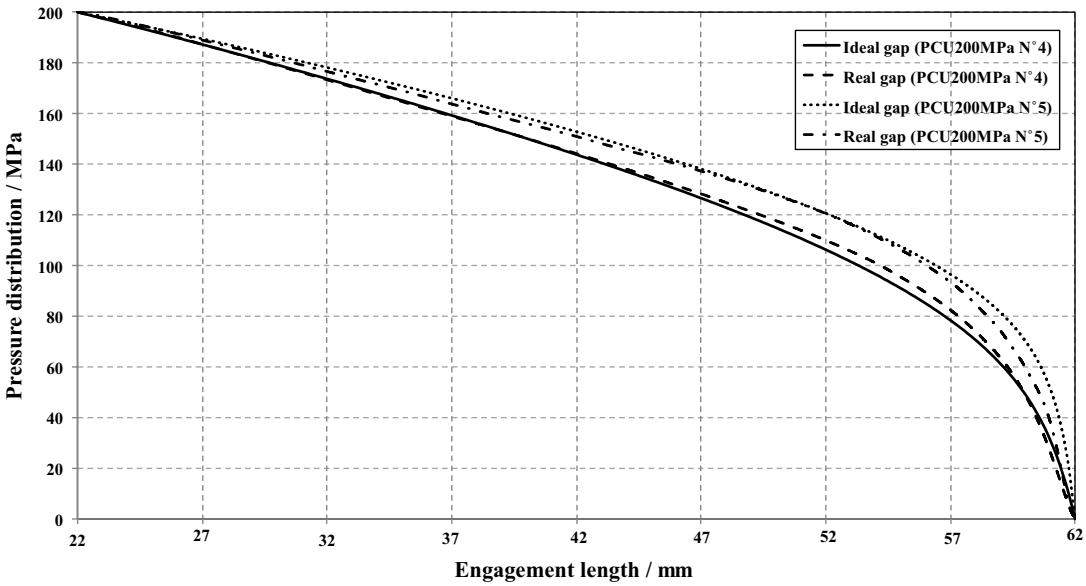

Figure 5. Pressure distribution for the ideal and real gaps between the piston and the cylinder in the FD mode for the 200 MPa PCUs N°4 and N°5 at $p = 200$ MPa.

Table 2. Pressure distortion coefficients and piston fall rates obtained for the ideal and real gaps and differences between them in the FD mode for the 200 MPa PCUs N°4 and N°5.

		$\lambda/10^{-7}$ MPa^{-1}			v_f/μm s^{-1}		
PCU	Pressure/MPa	Ideal gap	Real gap	$\Delta\lambda$	Ideal gap	Real gap	Δv_f
200 MPa N°4	20	8.10	7.85	0.25	0.227	0.226	0.001
	70	8.05	7.81	0.24	1.529	1.525	0.004
	120	8.05	7.91	0.14	3.736	3.723	0.013
	160	8.05	7.96	0.09	5.844	5.826	0.018
	200	8.05	7.99	0.06	8.016	7.993	0.023
200 MPa N°5	20	8.06	7.97	0.09	0.048	0.075	−0.027
	70	8.03	7.85	0.18	0.613	0.846	−0.233
	120	8.03	7.98	0.05	1.930	2.503	−0.573
	160	8.03	8.03	0.00	3.377	4.249	−0.872
	200	8.04	8.06	−0.02	4.989	6.150	−1.161

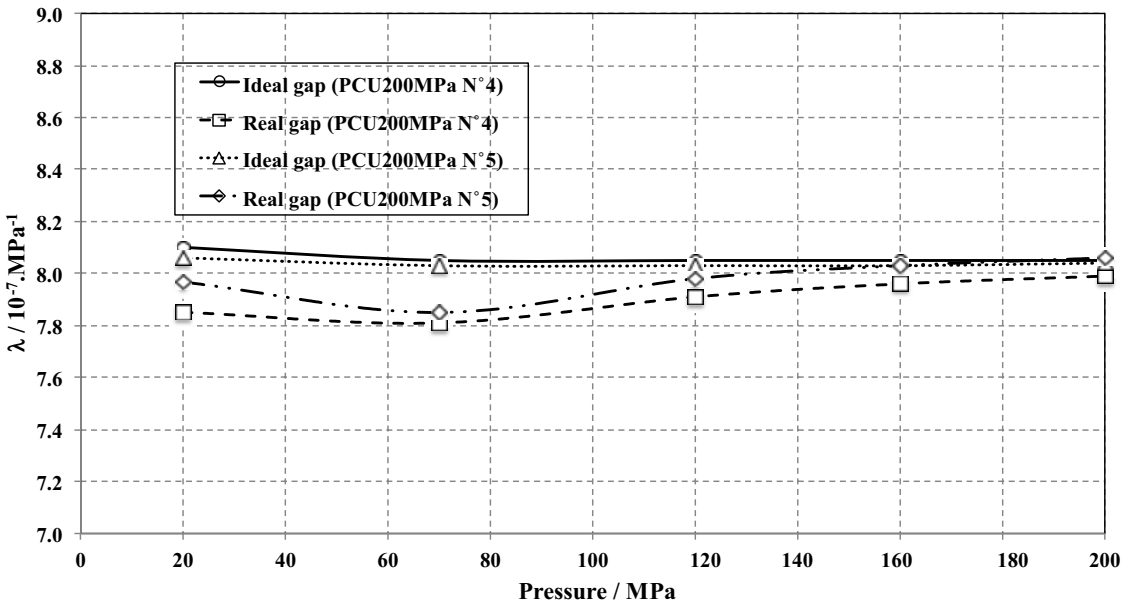

Figure 6. Pressure distortion coefficients calculated for the ideal and real gaps in the FD mode for the 200 MPa PCUs N°4 and N°5.

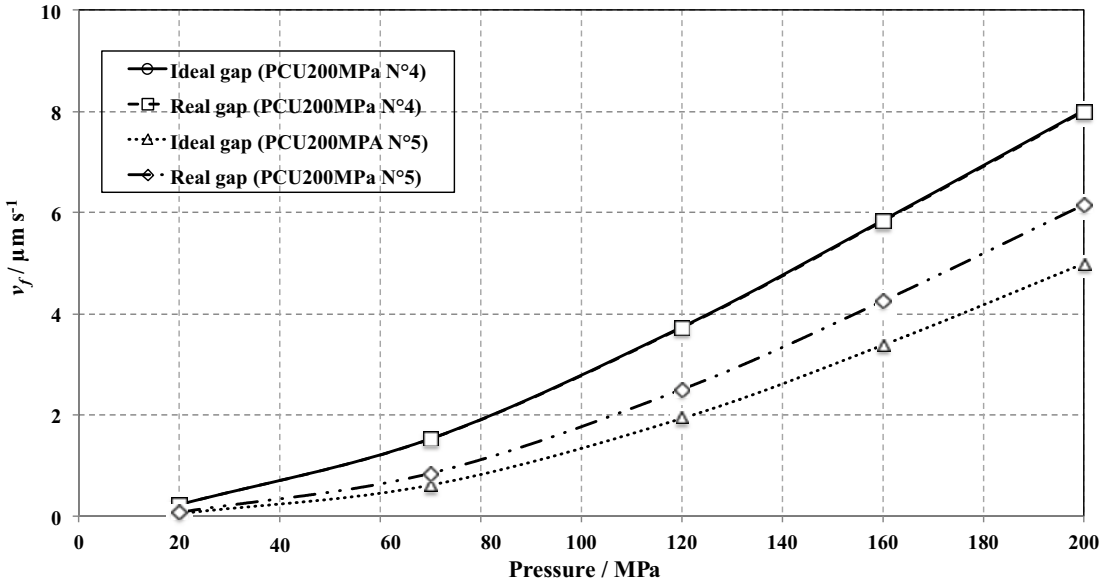

Figure 7. Piston fall rates obtained after calculating the ideal and real gaps in the FD mode for the 200 MPa PCUs N°4 and N°5.

Table 3. Main uncertainty sources, their contribution and combined standard uncertainty of the pressure distortion coefficient in the FD mode of the 200 MPa PCUs N°4 and N°5 (all values in units of 10^{-7} MPa^{-1}).

	200 MPa PCU N°4				200 MPa PCU N°5			
	Ideal gap		Real gap		Ideal gap		Real gap	
Uncertainty source	$p = 20$ MPa	$p = 200$ MPa	$p = 20$ MPa	$p = 200$ MPa	$p = 20$ MPa	$p = 200$ MPa	$p = 20$ MPa	$p = 200$ MPa
E_p	0.070	0.070	0.076	0.069	0.070	0.070	0.080	0.067
μ_p	0.026	0.026	0.026	0.026	0.026	0.026	0.026	0.026
E_c	0.27	0.27	0.26	0.27	0.27	0.27	0.26	0.27
μ_c	0.0090	0.0085	0.0085	0.0090	0.0090	0.0085	0.0085	0.0085
Gap width	0.0030	0.0015	0.045	0.0050	0.0050	0.000 50	0.074	0.022
Gap conicity	—	—	0.33	0.0065	—	—	1.21	0.036
Combined standard uncertainty	**0.28**	**0.28**	**0.43**	**0.28**	**0.28**	**0.28**	**1.24**	**0.28**

maximum difference of the piston fall rate obtained for the ideal and real gaps is $0.023\,\mu m\,s^{-1}$ for the 200 MPa PCU N°4 and $-1.161\,\mu m\,s^{-1}$ for the 200 MPa PCU N°5.

The results of the uncertainty analyses are summarized in table 3. It shows only the contributions that are significant for the combined uncertainty of the pressure distortion coefficient. These uncertainties were determined by simulating variations of each influence parameter in its estimated range of variation.

The uncertainty budgets obtained for the ideal gap profiles do not contain the gap conicity, which is an important uncertainty source for real gap profiles, in particular at low pressures. It could not be indicated that the uncertainty for ideal gap profiles is smaller than that for the real gap profiles. At high pressure, the combined standard uncertainty for ideal and real gap profiles is the same.

6. Conclusions

The pressure distortion coefficients with their uncertainties and the piston fall rates of 200 MPa PCUs N°4 and N°5 used for a pressure balance up to 200 MPa were determined by applying the ideal and real gap profiles. The results of two models were calculated by the newly developed finite element method. The ideal gap calculations of λ were not significantly different at different pressures. The calculation results of the real gap were dependent on the measured pressures but these differences fell within the uncertainty estimation. A comparison of the pressure distortion coefficients obtained for the ideal and real gap profiles indicated a maximum difference of $0.17 \times 10^{-7}\,MPa^{-1}$ and $0.06 \times 10^{-7}\,MPa^{-1}$ for the 200 MPa PCUs N°4 and N°5, respectively. This means that the ideal and real gap profiles do not have significant effect on the pressure distortion coefficient. The sensitivity of the uncertainty to the input quantities indicated that the Young modulus of the cylinder has a considerable effect on λ. The gap conicity of the real gap profile significantly influenced the λ calculations only at the low measured pressure.

The piston fall rates obtained for the ideal and real gap profiles were in good agreement for the 200 MPa PCU N°4 but not in good agreement for the 200 MPa PCU N°5. The results of the calculations showed that the piston fall rate is very sensitive to the gap profile and gap width and particularly to the gap properties in the gap inlet and outlet regions.

To understand the effect of the gap inlet and outlet on the piston fall rate calculations, the authors will focus on different methods to determine the cylinder radius at the top and bottom of the piston–cylinder engagement length, and the results will be compared with the experimental data.

References

[1] Buonanno G, Dell'Isola M and Maghenzani R 1999 Finite element analysis of pressure distortion coefficient and piston fall rate in a simple pressure balance *Metrologia* **36** 579–84

[2] Molinar G, Buonanno G, Giovinco G, Delajoud P and Haines R 2005 Effectiveness of finite element calculation methods (FEM) on high performance pressure balance in liquid media up to 200 MPa *Metrologia* **42** S207–11

[3] Rabault T and Legras J C 2005 Calculation of the pressure distortion coefficient and uncertainty budget of the BNM/LNE national standard *Metrologia* **42** S246–9

[4] Buonanno G, Man J and Molinar Min Beciet G 2007 Characterization of the IMGC-DH100L pressure balance using finite element analysis *IMEKO 20th TC3, 3rd TC16 and 1st TC22 International Conf. (Mérida, Mexico, November 2007)*

[5] Molinar G, Sabuga W, Robinson G and Legras J C 1998 Comparison of methods for calculating distortion in pressure balances up to 400 MPa—EUROMET Project 256 *Metrologia* **35** 739–59

[6] Sabuga W, Molinar G, Buonanno G, Esward T, Legras J C and Yagmur L 2006 Finite element method used for calculation of the distortion coefficient and associated uncertainty of a PTB 1 GPa pressure balance—EUROMET Project 463, *Metrologia* **43** 311–25

[7] Vergne P 1990 New high pressure viscosity measurements on di(2-ethylhexyl) sebacate and comparison with previous data *High Temp. High Pressure* **22** 613–21

[8] Yavorski B and Detlaf A 1975 *Aide-Mémoire de Physique* 3rd edn (Moscow: Mir) pp 328–55

[9] Dadson R S, Lewis S L and Peggs G N 1982 *The Pressure Balance: Theory and Practice* (London: HMSO)